

Estimating Forest Net Primary Productivity Using Two Seasonal SPOT Images

Chi-Chuan Cheng^{1,2)}

[Summary]

This study aimed to apply remote sensing to estimate the forest net primary productivity (NPP) of Nanzhuang National Forest in Taiwan. The research processes included calculating vegetation indices from SPOT images of 2 seasons in 2003, estimating the fraction of photosynthetically active radiation (FPAR) and photosynthetically active radiation absorbed by the different forest types (APAR), estimating the NPP, and finally analyzing NPP variations from different seasons and forest types. Furthermore, the shadow effect, simulation of the maximum light use efficiency for different forest types, and the problem of image acquisition for NPP estimation in Taiwan were also investigated. The results are as follows. Under the consideration of the shadow effect and simulation of the maximum light use efficiency for different forest types, the NPP estimation on the dry season image was $361.22 \text{ g C m}^{-2} \text{ yr}^{-1}$ with shadow retention and $293.19 \text{ g C m}^{-2} \text{ yr}^{-1}$ with shadow correction, while the wet season image was $545.07 \text{ g C m}^{-2} \text{ yr}^{-1}$ with shadow retention and $572.45 \text{ g C m}^{-2} \text{ yr}^{-1}$ with shadow correction. As for using dry- and wet-season images, NPP values were 452.5 and $432.43 \text{ g C m}^{-2} \text{ yr}^{-1}$ with shadow retention and shadow correction, respectively. A comparison between the estimated NPP and the field-measured carbon amount derived from forest inventory data (i.e., $430 \text{ g C m}^{-2} \text{ yr}^{-1}$) indicated that the NPP estimated from 2 seasonal images had the best result because of the smallest bias. Meanwhile, the seasonal analysis of NPP variations was significant in the study area. The majority of NPP accumulation was about 86% of the annual NPP and was mainly distributed between April and October. In addition, we propose that among the 3 shadow processes, shadow removal cannot be applied to estimate the NPP because a lower FPAR was generated when estimating the FPAR due to the linear transformation of vegetation indices. We concluded that remote sensing is a timely, effective, feasible, and large-scale approach for estimating the forest NPP and provides the NPP for a spatiotemporal variation analysis. Meanwhile, the shadow effect and simulation of the maximum light use efficiency for forest types affect the estimation of forest NPP. Therefore, their effects should be considered when applying SPOT vegetation indices to estimate forest NPP. In addition, an alternative approach using seasonal images is also feasible to eliminate the problem with image acquisition in Taiwan.

Key words: net primary productivity, remote sensing, vegetation indices.

Cheng CC. 2014. Estimating forest net primary productivity using two seasonal SPOT images. Taiwan J For Sci 29(4):251-66.

¹⁾ Department of Landscape Architecture, Chinese Culture Univ., 55 Hwakang Rd., Taipei 11114, Taiwan. 中國文化大學景觀學系，11114台北市華岡路55號。

²⁾ Corresponding author, e-mail: zqq@faculty.pccu.edu.tw 通訊作者。

Received December 2013, Accepted October 2014. 2013年12月送審 2014年10月通過。

研究報告

森林淨初級生產力之遙測估算

鄭祈全^{1,2)}

摘要

本研究目的主要在藉由遙測技術，估算南庄事業區之森林淨初級生產力(NPP)。研究過程包括2003年SPOT衛星影像之植生指數計算、光合作用有效輻射分量(FPAR)和光合作用有效吸收輻射(APAR)之估算、森林淨初級生產力之估算、以及不同季節和不同林型之淨初級生產力的變化分析，進而探討影像陰影、林型最大光能利用率模擬、及影像獲取等問題對森林NPP估算之影響。研究結果指出，在考量影像陰影和林型最大光能利用率模擬的情況之下，SPOT乾季影像在陰影保留和陰影校正處理後所估算的NPP分別為361.22和293.19 g C m⁻² yr⁻¹；溼季影像為545.07和572.45 g C m⁻² yr⁻¹；而使用乾、溼二季影像所估算的NPP則為452.5和432.43 g C m⁻² yr⁻¹。上述應用遙測方法估算的NPP，經與地面樣區調查方法所得的結果(430 g C m⁻² yr⁻¹)比較後顯示，使用乾、溼二季影像因差值最小，估算結果較佳，其中又以經陰影校正處理的結果最佳。同時，從NPP季節變化的分析結果得知，NPP的積累期主要發生在4~10月份，約占了年淨初級生產力總量的86%。其次，本研究在執行陰影處理過程中亦發現，使用陰影移除的作法並不適合於NPP之遙測估算，其原因主要是植生指數會因線性轉換而造成FPAR估算值變小，並導致NPP估算值偏低的現象。

由上述研究結果可得結論如下：應用遙測技術估算森林NPP，除了具有即時、有效、經濟、可行和大尺度的特性之外，並可提供森林NPP時空動態變化分析之用。但因影像陰影和林型最大光能利用率問題會影響森林NPP之估算，因此在應用SPOT植生指數估算NPP時，必須考量其影響效應。此外，台灣因環境關係，較難獲取逐月的SPOT衛星影像，供森林NPP估算之用。針對此問題，本研究使用SPOT季節性影像進行NPP估算的作法，可提供影像獲取不易但乾、溼季分明的地區做為參考。

關鍵詞：淨初級生產力、遙測、植生指數。

鄭祈全。2014。森林淨初級生產力之遙測估算。台灣林業科學29(4):251-66。

INTRODUCTION

Global climate change has been an issue of growing concern since the end of the 20th century. The increasing amount of carbon dioxide is regarded as one of the important factors accelerating global warming and leading to global climate change. Therefore, many countries signed the Kyoto Protocol (KP) in 1997. The KP agreed that carbon sequestration can reduce climate change, and participating nations are required to estimate their greenhouse gases and provide a national greenhouse gas inventory report. Since then,

carbon sequestration has become an important issue in terms of absorbing and storing carbon dioxide. Meanwhile, forests play important roles because they yield the greatest potential for reducing greenhouse gas emissions. Several studies indicated that the combination of forest inventories and remote sensing has become the main method for assessing carbon amounts. Particularly, according to the International Panel on Climate Change (IPCC) Good Practice Guidance, remote sensing is a useful technique for estimating carbon

amounts on a large scale to verify national land uses, land-use changes, and forestry (LULUCF).

As for estimating carbon amounts, several methods have been proposed, including sampling of ground biomass, flux towers, model estimation, and remote sensing techniques. Among these methods, remote sensing is an effective and large-scale method for estimating net primary productivity (NPP) (Zhu 2005). Common approaches used in remote sensing are regression models of forest stocks and vegetation indices to estimate carbon amounts (Monteith 1972, Wang 2010). Several studies applied different scales of remote sensing images to estimate the NPP and analyze changes in NPP (Law and Waring 1994, Raymond and Hunt 1994, Goetz and Prince 1996, Gower et al. 1999, Zhu 2005). However, the shadow effect and simulation of the maximum light use efficiency (ϵ_{\max}) for vegetation types must be considered when estimating the NPP (Burgess et al. 1995, Zhu et al. 2006). For example, the shadow effect in high-relief areas affects the amounts of red and infrared radiation reflected by the land surface. Burgess et al. (1995) investigated the shadow effect on AVHRR NDVI data with a digital elevation model to simulate the shadow effect. They found shadow errors of as large as 13.5% at a 50-m resolution which became smaller with an increasing pixel size; for pixels of 1.1-km resolution, the error was < 3%. Therefore, Burgess et al. (1995) concluded that the fairly strong shadow effect in high-resolution data is greatly reduced in low-resolution data. In addition to the shadow effect, the ϵ_{\max} is also a key parameter for estimating NPP when applying remote sensing data. However, many divergences still exist as to its value with different vegetation types (Potter et al. 1993, Field et al. 1995, Peng et al. 2000, Zhu et al. 2006). Potter et al. (1993)

and Field et al. (1995) took the global ϵ_{\max} to be 0.389 g C MJ⁻¹. Peng et al. (2000) adopted 1.25 g C MJ⁻¹ to estimate the spatial distribution of the ϵ_{\max} in Guangdong Province, China and indicated the ϵ_{\max} used in the CASA model (0.389 g C MJ⁻¹) was lower compared to that of Guangdong vegetation. For this reason, Zhu et al. (2006) simulated the ϵ_{\max} for some typical vegetation types in China based on NOAA/AVHRR remote sensing data and field-observed NPP data. From previous research, values of the ϵ_{\max} for different vegetation types were obviously inconsistent.

Due to the importance of forest NPP and the potential use of remote sensing, this study applied SPOT images to estimate the NPP of Nanzhuang National Forest in Taiwan and also examined the shadow effect and ϵ_{\max} for estimating NPP. However, another problem also exists in Taiwan, that is, monthly images are needed to estimate the annual NPP when using remote sensing. In fact, it is difficult to acquire monthly SPOT images in Taiwan due to the environmental characteristics. Therefore, seasonal SPOT images were applied in this study to investigate their feasibility for NPP estimation.

MATERIALS AND METHODS

Study area

Nanzhuang National Forest, which belongs to the Taiwan Forest Bureau, is located in northern Taiwan (Fig. 1). The area covers about 9129.36 ha, and the elevation ranges 145~2610 m. The mean temperature ranges 15.1~28.8°C. The mean annual rainfall is about 1782.7 mm yr⁻¹.

Materials

Remote sensing data

As mentioned previously, it is difficult to acquire monthly SPOT images for NPP

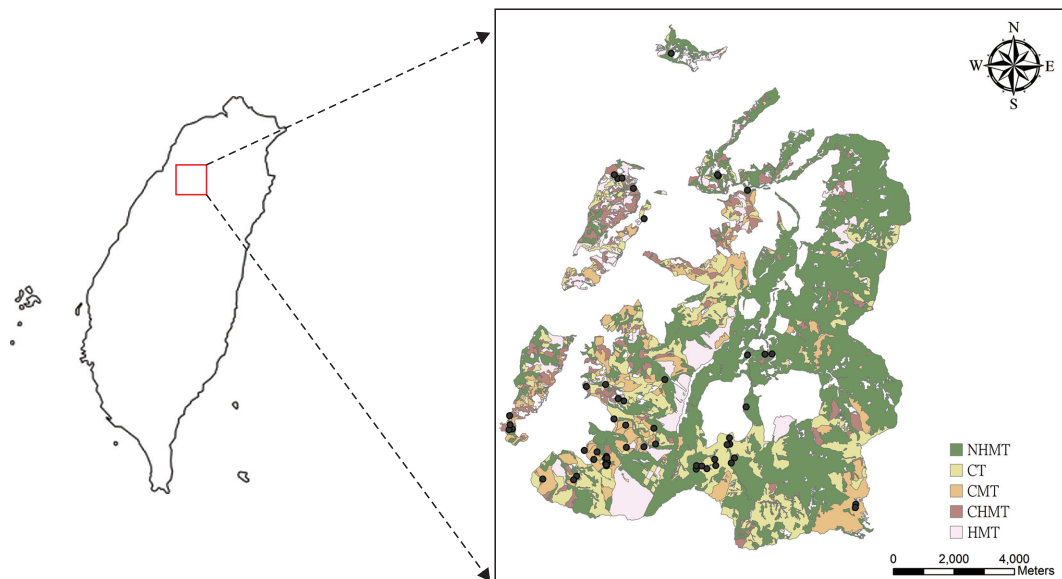


Fig. 1. Study area and forest type map including natural hardwood mixed type (NHMT), conifer type (CT), conifer mixed type (CMT), conifer-hardwood mixed type (CHMT), hardwood mixed type (HMT). Black points denote the 55 field plots.

estimation in Taiwan. However, there are distinct dry and wet seasons. Therefore, according to the meteorological data including total monthly precipitation, mean monthly temperature, and total monthly solar radiation, 2 clear SPOT-4 images acquired on 2003 January 17 and 2003 June 28 were selected from the Center for Space and Remote Sensing Research (CSRSR), National Central University, Jhongli City, Taiwan. The SPOT images included green (0.5~0.59 μm), red (0.61~0.68 μm), infrared bands (0.79~0.89 μm), and short-wave infrared (SWIR, 1.58~1.75 μm) with a 20 \times 20-m spatial resolution, and have precision correction with ground control points and digital terrain model (DTM). To examine the feasibility of seasonal images for NPP estimation in this study, the 2 available SPOT images were assumed to be representative of the dry (2003 January 17) and wet seasons (2003 June 28) according to the meteorological data.

Meteorological data

To acquire meteorological data of the study area in 2003, total monthly precipitation, mean monthly temperature, and total monthly solar radiation in Taiwan were provided by the Taiwan Typhoon and Flood Research Institute and derived from 392, 122, and 22 meteorological stations, respectively. All data were compiled with missing and suspicious data, and then interpolated at the same scale with the SPOT images using the geostatistical analysis of ArcGIS 10.2 software (Environmental System Research Institute, Inc.). After that, 3 kinds of monthly meteorological data of the Nanzhuang National Forest were further extracted from Taiwan's monthly meteorological data.

Forest type map, field inventory data of plots, and field-measured carbon amounts

The forest type map (Fig. 1) and field inventory data of Nanzhuang National Forest

were collected from the Taiwan Forest Bureau. The forest type map is classified into 5 types: natural hardwood mixed type (NHMT), conifer type (CT), conifer mixed type (CMT), conifer-hardwood mixed type (CHMT), and hardwood mixed type (HMT). The field inventory data included 55 plots. The relationship between the forest type and number of plots was as follows: NHMT=18, CT=10, CMT=15, CHMT=8, and HMT=4. As for the plot size, there were 3 kinds of rectangular plot sizes: 40×25 m (0.1 ha), 28.4×17.6 m (0.05 ha), and 17.9×11.2 m (0.02 ha). Each plot had been inventoried in 1998 and 2003. The inventory data included tree species, diameter at breast (DBH), and tree height (H). As for the field-measured carbon amount based on forest inventory data, the Timber Resources Inventory Projection System (TRIPS) established by the Taiwan Forest Bureau was used. There are 3 steps as follows. (1) Calculation of forest stocks was based on forest inventory data in 1998 and 2003. Only 52 field plots were used to calculate forest stock due to 3 missing plots in 1998. The forest stock of each plot was first calculated using the TRIPS and a stock equation of the Taiwan Forest Bureau. Then this was converted from

plot size into per hectare, and the forest stock was further estimated for each forest type. (2) The forest carbon stock for each forest type was then estimated using the calculated forest stock by the following equation (1):

$$C = V_{\text{stem/ha}} \times EF \times D \times CF; \quad (1)$$

where C is the carbon stock per hectare, $V_{\text{stem/ha}}$ is the forest stock per hectare, EF is the expansion factor from stem stock to tree stock, D is the density from forest stock to biomass, and CF is the carbon fraction.

In equation (1), a couple of parameters refer to the IPCC (Wang 2007). For example, the expansion factor (EF) was assumed to be 1.65 while the carbon fraction (CF) was 0.5. As for the parameter of density (D), 5 forest types (i.e., NHMT, CT, CMT, CHMT, and HMT) were assumed to be 0.49, 0.44, 0.44, 0.46, and 0.49, respectively (Wang 2010). (3) The field carbon amount of 2003 was finally measured according to the estimated forest carbon stocks in 1998 and 2003. Table 1 shows the results of field-measured carbon amounts for 2003.

Methodology

Figure 2 is a flow chart for NPP estimation based on SPOT vegetation indices. The

Table 1. Field-measured carbon amount of the Nanzhuang National Forest in 2003 according to the inventory data of field plots

Forest type	NHMT	CT	CMT	CHMT	HMT	Study area
Area (ha)	5008.13	1663.67	927.13	677.29	853.14	9129.36
No. of plots	18	9	14	8	3	52
Forest stock in 1998 (m ³ ha ⁻¹)	236.83	670.09	193.55	238.41	205.01	308.78
Forest stock in 2003 (m ³ ha ⁻¹)	282.24	734.83	294.37	283.66	256.86	390.98
Carbon stock in 1998 (g C m ⁻²)	9991	20523	5426	8636	10546	11024
Carbon stock in 2003 (g C m ⁻²)	12030	22478	8218	11002	12841	13314
Carbon stock in 5 yrs (g C m ⁻²)	2039	1955	2792	2366	2295	2290
Carbon amount (g C m ⁻² yr ⁻¹)	408	391	558	473	459	430
Total carbon (10 ⁶ g C yr ⁻¹)	20433.17	6504.95	5173.39	3203.58	3915.91	39231.00

NHMT, natural hardwood mixed type; CT, conifer type; CMT, conifer mixed type; CHMT, conifer-hardwood mixed type; HMT, hardwood mixed type.

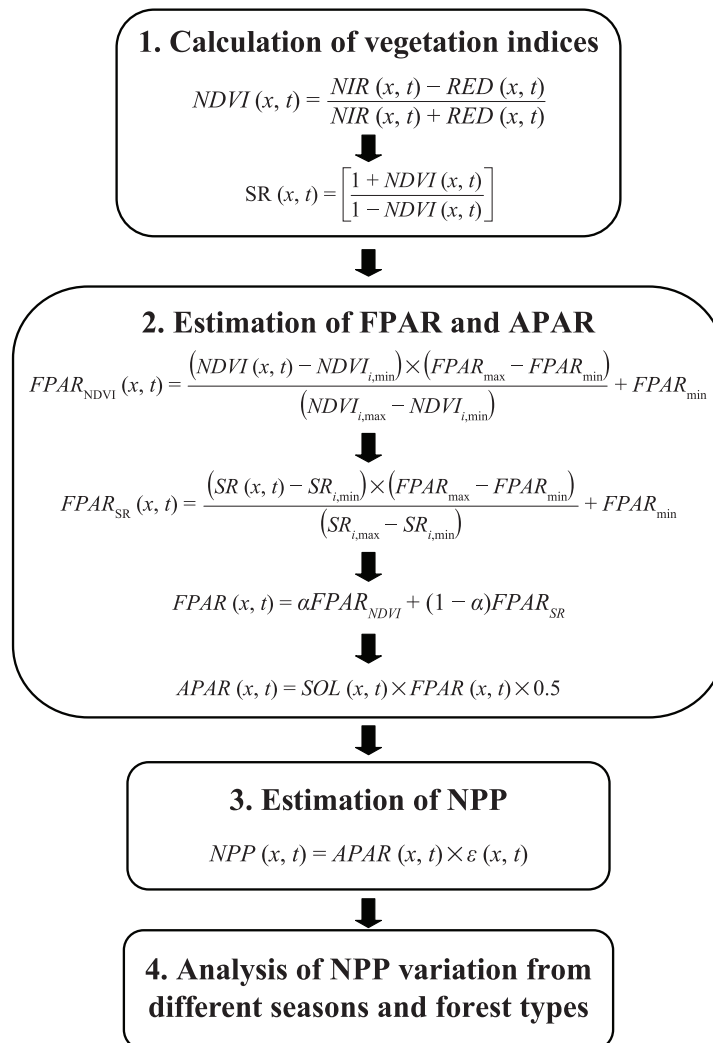


Fig. 2. Flow chart for estimating forest net primary productivity (NPP).

(NDVI, Normalized Difference Vegetation Index; SR, Simple Ratio Vegetation Index; FPAR, Fraction of Photosynthetically Active Radiation; APAR, Absorbed Photosynthetically Active Radiation; SOL, Solar Radiation)

research process included calculating vegetation indices from the SPOT image, estimating the fraction of photosynthetically active radiation (FPAR) and photosynthetically active radiation absorbed (APAR) by forest types, estimating NPP, and finally analyzing NPP variations in different seasons and forest types. In addition, common problems occurring in Taiwan were also investigated. For ex-

ample, the shadow effect, ϵ_{max} for forest types, and image acquisition on the estimation of forest NPP were examined.

Calculation of the vegetation index from SPOT images with shadow processes

The Normalized Difference Vegetation Index (NDVI) and Simple Ratio Vegetation Index (SR) were used in this study, because

both indices are primary parameters for estimating the FPAR (Los et al. 1994). The NDVI is commonly applied to vegetation indices. This was calculated with the near-infrared (NIR) and red (RED) bands as shown in equation (2). The NDVI range is between -1 and 1, meaning there is high-density vegetation when it is close to 1. On the other hand, the land-use type is non-vegetation when the NDVI is < 0.

$$NDVI(x, t) = \frac{NIR(x, t) - RED(x, t)}{NIR(x, t) + RED(x, t)}, \quad (2)$$

where x is a pixel in the SPOT image, and t is the period of the image.

The SR was calculated by the NDVI as in equation (3). The index represents the richness of vegetation, but is affected by region and seasonality.

$$SR(x, t) = \left[\frac{1 + NDVI(x, t)}{1 - NDVI(x, t)} \right]. \quad (3)$$

According to a previous report (Zhou et al. 2009), vegetation indices are affected by image shadows. To deal with this problem in this study, a shadow map was first generated by unsupervised classification under the ISO-DATA (Iterative Self-Organizing Data Analysis Technique) clustering method of ERDAS IMAGINE software (Intergraph Corporation). Then the shadow map with 55 field plots was overlaid, and shadow processes were carried out, such as shadow retention, shadow removal, and shadow linear-correlation correction. Equation (4) is the shadow linear-correlation correction for adjusting the NDVI:

$$DN_{stretch} = \frac{[Shadow_{SD}]}{(NonShadow_{SD})} \times (DN_{shadow} - Shadow_{M}) + NonShadow_{SD}; \quad (4)$$

where $DN_{stretch}$ and DN_{shadow} represent the NDVI value with and without shadow correction, $Shadow_{SD}$ and $NonShadow_{SD}$ are the standard deviations of NDVI in shadow and non-shadow forestland, and $Shadow_{M}$ and

$NonShadow_{M}$ refer to the NDVI in shadow and non-shadow forestland, respectively.

Estimations of FPAR and APAR with seasonal images

According to previous research (Hatfield et al. 1984, Sellers 1985), the relation between FPAR and NDVI is near-linear. Therefore, the relation of FPAR and NDVI can be used to estimate the FPAR of NDVI (i.e., $FPAR_{NDVI}$) if linearity is assumed. The equation between FPAR and NDVI is given by

$$FPAR_{NDVI}(x, t) = \frac{(NDVI(x, t) - NDVI_{i,min}) \times (FPAR_{max} - FPAR_{min})}{(NDVI_{i,max} - NDVI_{i,min})} + FPAR_{min}; \quad (5)$$

where $FPAR_{max} = 0.950$ and $FPAR_{min} = 0.001$ are based on research by Hatfield et al. (1984) and Sellers (1985). Both are independent of vegetation types.

In addition to the above $FPAR_{NDVI}$, Los et al. (1994) and Field et al. (1995) also indicated that the FPAR has a linear relationship with the SR. The relation between the FPAR and SR (i.e., $FPAR_{SR}$) is as in equation (6):

$$FPAR_{SR}(x, t) = \frac{(SR(x, t) - SR_{i,min}) \times (FPAR_{max} - FPAR_{min})}{(SR_{i,max} - SR_{i,min})} + FPAR_{min}; \quad (6)$$

where $SR_{i,max}$ and $SR_{i,min}$ respectively correspond to the $NDVI_{i,max}$ and $NDVI_{i,min}$.

To understand which model is suitable for estimating the FPAR, a comparison was made between the $FPAR_{NDVI}$ and $FPAR_{SR}$ (Los et al. 1994). Results indicated that a large bias existed in the $FPAR_{NDVI}$, while a smaller bias occurred in the $FPAR_{SR}$. To resolve this problem, Los et al. (1994) took the model as in equation (7), and found that the mean FPAR estimated by the $FPAR_{NDVI}$ (equation 5) and $FPAR_{SR}$ (equation 6) had the smallest bias. Therefore, according to the research results of

Los (1998), this study adopted equation (7) to estimate the FPAR with α arbitrarily set to 0.5: $FPAR(x, t) = \alpha FPAR_{NDVI}(x, t) + (1 - \alpha) FPAR_{SR}(x, t)$. (7)

After the FPAR estimation, the APAR ($MJ\ m^{-2}\ mo^{-1}$) was further estimated. It is the product of PAR and FPAR at each monthly time step. Based on the research of Zhu (2005), the PAR equals half of the total solar radiation (SOL) ($MJ\ m^{-2}$) in this study. The APAR is then given by

$$APAR(x, t) = SOL(x, t) \times FPAR(x, t) \times 0.5. \quad (8)$$

As mentioned previously, the effect of image acquisition on NPP estimations was also investigated in this study. Therefore, in addition to the FPAR of the dry and wet seasons, this study also used the average of the mean FPAR of the dry and wet seasons as the $FPAR_{AVERAGE}$ for estimating the APAR and NPP. The objective was to investigate the feasibility of using seasonal images for NPP estimations.

Estimation of NPP

NPP ($g\ C\ m^{-2}\ mo^{-1}$) is the product of APAR and the actual light use efficiency (ϵ) ($g\ C\ MJ^{-1}$) at each monthly time step:

$$NPP(x, t) = APAR(x, t) \times \epsilon(x, t). \quad (9)$$

As for the ϵ in equation (9), Potter et al. (1993) and Field et al. (1995) indicated the ϵ is affected by temperature and water. It is the product of the ϵ_{max} ($g\ C\ MJ^{-1}$) and the scales representing the availability of water (W) and the suitability of temperature (T_1, T_2), as shown in equation (10):

$$\epsilon(x, t) = W(x, t) \times T_1(x, t) \times T_2(x, t) \times \epsilon_{max}. \quad (10)$$

Here, ϵ_{max} means each forest type has a maximum light use efficiency in an ideal condition. The water scalar is a function of the ratio of the estimated evapotranspiration (E) to potential evapotranspiration (E_p) at each

monthly time step as shown in equation (11). As for the calculation of W , this study referred to Zhu (2005) and adopted the concept of regional estimated evapotranspiration and regional potential evapotranspiration to calculate the W :

$$W(x, t) = 0.5 + 0.5 \times E(x, t) / E_p(x, t). \quad (11)$$

The 2 temperature scalars represent the regulation of plant growth by temperature. The values of T_1 and T_2 were calculated by equations (12) and (13):

$$T_1(x, t) = 0.8 + 0.02 \times T_{opt}(x) - 0.0005 \times [T_{opt}(x)]^2 \text{ and} \quad (12)$$

$$T_2(x, t) = \frac{1.184}{\{1 + \exp[0.2 \times (T_{opt}(x) - 10 - T(x, t))]\}} \times \frac{1}{\{1 + \exp[0.3 \times (-T_{opt}(x) - 10 + T(x, t))]\}}; \quad (13)$$

where $T_{opt}(x)$ is the mean monthly temperature with the maximum NDVI in a year.

Finally, equations (9) and (10) were combined into the model as equation (14):

$$NPP(x, t) = APAR(x, t) \times W(x, t) \times T_1(x, t) \times T_2(x, t) \times \epsilon_{max}. \quad (14)$$

The ϵ_{max} in equation (14) is a key parameter for estimating NPP in remote sensing applications. Related research about simulating ϵ_{max} for forest types is rare in Taiwan. Therefore, this study proposed simulating the ϵ_{max} according to the known parameters of APAR, T_1, T_2, W , and field-measured carbon amount (Table 1) in 2003. After the simulated ϵ_{max} was generated, equation (14) was applied to estimate the monthly NPP of each forest type. Finally, the monthly NPP was accumulated into the annual NPP ($g\ C\ m^{-2}\ yr^{-1}$) of the study area in 2003.

Analysis of NPP variations from different seasons and forest types

After estimating NPP, NPP variations were further analyzed from different seasons and forest types. The analysis from different

seasons focused on the accumulation period of NPP and variations among the 4 seasons (i.e., spring, summer, autumn, and winter). As for NPP variations in different forest types, the analysis focused on spatial variations of 5 forest types (i.e., NHMT, CT, CMT, CHMT, and HMT) under the processes of shadow retention and shadow correction.

RESULTS AND DISCUSSION

Calculation of NDVI and SR with shadow processes

Unsupervised classification using the ISODATA clustering method of ERDAS IMAGINE software was first applied to generate shadow maps for the dry (2003 January 17) and wet seasons (2003 June 28) as shown in Fig. 3. The generated shadow map was then overlaid onto the original SPOT image for further interpretation of the shadow area. The results indicated that the dry- and wet-season images were covered by about 21.9 and 15.8% shadow areas, respectively.

The effects of shadow processes (i.e., shadow retention, shadow removal, and shadow linear-correlation correction) on the NDVI and SR values were further investigated. Results are shown in Table 2. Clearly, the mean NDVI or SR in the dry-season image was smaller than that of the wet-season image. However, from the shadow effect on the NDVI or SR, shadow removal was larger than shadow retention and very close to the shadow correction for the dry- or wet-season image.

Estimation of the FPAR and APAR with shadow processes and seasonal images

Similar to the process of NDVI and SR calculation, dry- and wet-season images were applied to estimate the mean FPAR with shadow processes. The results are shown in Table 3 and summarized as follows. (i) The mean of $FPAR_{NDVI}$ was larger than that of $FPAR_{SR}$ regardless of the shadow process or seasonal image. This differed from the NDVI and SR (Table 2). (ii) The means of $FPAR_{NDVI}$, $FPAR_{SR}$, $FPAR$ derived from the

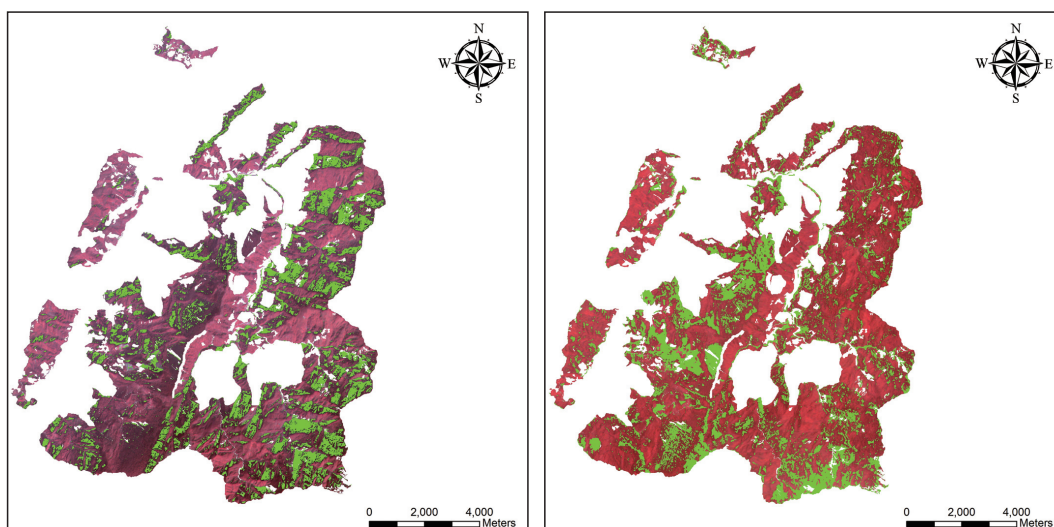


Fig. 3. SPOT images on 2003 January 17 (left) and 2003 June 28 (right). The green color denotes shadow areas.

Table 2. Means of Normalized Difference Vegetation Index (NDVI) and Simple Ratio Vegetation Index (SR) with shadow processes and seasonal images

Indices	2003 January 17 (dry season)			2003 June 28 (wet season)		
	Shadow retention	Shadow removal	Shadow correction	Shadow retention	Shadow removal	Shadow correction
Mean of NDVI	0.4207	0.4717	0.4727	0.5223	0.5466	0.5475
Mean of SR	2.6988	2.9432	2.9208	3.2483	3.4443	3.4520

Table 3. Mean fraction of photosynthetically active radiation (FPAR) with shadow processes and seasonal images

Types	2003 January 17 (dry season)			2003 June 28 (wet season)		
	Shadow retention	Shadow removal	Shadow correction	Shadow retention	Shadow removal	Shadow correction
Mean of FPAR _{NDVI}	0.5160	0.4120	0.4122	0.7023	0.2917	0.7262
Mean of FPAR _{SR}	0.2432	0.2078	0.2042	0.4498	0.2024	0.4840
Mean of FPAR	0.3796	0.2088	0.3081	0.5762	0.2470	0.6051

NDVI, Normalized Difference Vegetation Index; SR, Simple Ratio Vegetation Index.

dry-season image were smaller than those derived from the wet-season image, except for the process of shadow removal. (iii) The means of FPAR_{NDVI}, FPAR_{SR}, and FPAR with shadow removal were pretty small compared to shadow retention or shadow correction, particularly in the wet-season image. The reason was due to the linear transformation of the FPAR.

From the third point of the above summary, there is an important implication, i.e., the mean FPAR with shadow removal has to be ignored, because the lower value of the FPAR can affect estimations of the APAR and NPP. Therefore, only 2 shadow processes (i.e., shadow retention and shadow correction) were used to estimate the APAR. Table 4

shows results of the mean FPAR with 2 shadow processes and seasonal images, including the FPAR in the dry and wet seasons, and the FPAR_{AVERAGE} in the dry and wet seasons. Figure 4 shows the means of the monthly APAR in dry- and wet-season images with shadow retention and shadow correction.

Estimation of the NPP with shadow processes and seasonal images

Simulation of the ϵ_{\max} for forest types

The ϵ_{\max} is a key parameter for estimating NPP derived from remote sensing data. Therefore, before estimating the NPP, this study applied equation (14) to simulate the ϵ_{\max} for each forest type of the study area according to the following known parameters:

Table 4. Mean fraction of photosynthetically active radiation (FPAR) with 2 shadow processes and seasonal images

Types	Shadow retention	Shadow correction
Mean of FPAR in the dry season	0.3796	0.3081
Mean of FPAR in the wet season	0.5762	0.6051
Mean of FPAR _{AVERAGE} in the dry and wet seasons	0.4779	0.4566

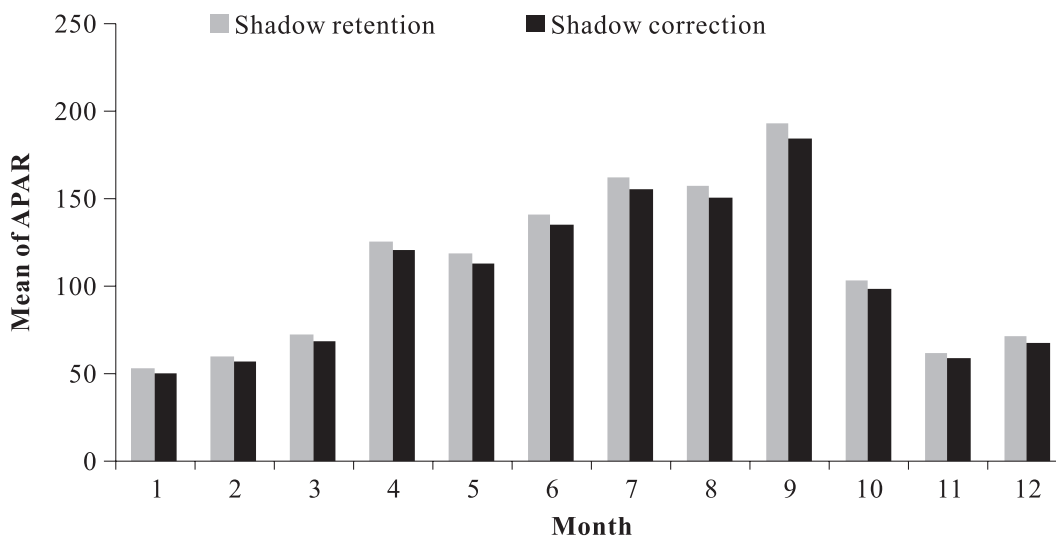


Fig. 4. Means of the monthly photosynthetically active radiation absorbed (APAR) by the different forest types in the dry- and wet-season images with 2 shadow processes.

(i) calculated T_1 , T_2 , and W parameters from meteorological data, (ii) the estimated APAR parameter from 2 seasonal images, and (iii) the field-measured carbon amount from the inventory data of field plots (Table 1). Table 5 shows the value of ϵ_{\max} for each forest type with shadow retention and shadow correction. The results indicated the ϵ_{\max} with shadow correction was larger than that with shadow retention. Therefore, this study applied the ϵ_{\max} with shadow correction to estimate the NPP because shadow correction was 1 objective of this study, and it really improved the NDVI (Table 2).

NPP estimations with shadow processes and seasonal images

Based on the known parameters of APAR, T_1 , T_2 , and W and the simulated ϵ_{\max} for each forest type, equation (14) was then applied to estimate monthly and annual NPP values with shadow processes and seasonal images. Results are shown in Table 6 and summarized as follows. First, annual NPP values estimated from the dry-season image were $361.22 \text{ g C m}^{-2} \text{ yr}^{-1}$ with shadow retention and $293.19 \text{ g C m}^{-2} \text{ yr}^{-1}$ with shadow correction. As for the wet-season image, annual NPP values were $545.07 \text{ g C m}^{-2} \text{ yr}^{-1}$ with

Table 5. Simulation of the maximum light use efficiency (ϵ_{\max}) with shadow retention and shadow correction

Forest type	ϵ_{\max} with shadow retention (unit: g C MJ^{-1})	ϵ_{\max} with shadow correction (unit: g C MJ^{-1})
NHMT	0.388	0.406
CT	0.386	0.404
CMT	0.555	0.580
CHMT	0.433	0.453
HMT	0.436	0.456

NHMT, natural hardwood mixed type; CT, conifer type; CMT, conifer mixed type; CHMT, conifer-hardwood mixed type; HMT, hardwood mixed type.

Table 6. Net primary productivity (NPP) in 2003 with shadow processes and seasonal images

Month	Dry-season image (g C m ⁻² yr ⁻¹)		Wet-season image (g C m ⁻² yr ⁻¹)		Dry- and wet- season images (g C m ⁻² yr ⁻¹)	
	Shadow retention	Shadow correction	Shadow retention	Shadow correction	Shadow retention	Shadow correction
January	7.91	6.39	11.84	12.44	9.84	9.40
February	10.09	8.15	15.14	15.91	12.58	12.02
March	15.90	12.87	23.89	25.10	19.84	18.96
April	37.78	30.64	56.93	59.80	47.26	45.17
May	34.05	27.62	51.40	53.98	42.68	40.78
June	48.53	39.42	73.20	76.86	60.75	58.06
July	50.45	40.93	76.19	80.02	63.26	60.45
August	53.79	43.68	81.20	85.27	67.40	64.41
September	60.09	48.96	90.90	95.41	75.39	72.05
October	25.89	20.97	39.15	41.14	32.54	31.09
November	9.87	8.00	14.92	15.68	12.40	11.85
December	6.88	5.55	10.32	10.84	8.57	8.19
Annual NPP	361.22	293.19	545.07	572.45	452.50	432.43

shadow retention and 572.45 g C m⁻² yr⁻¹ with shadow correction. Second, annual NPP values estimated from the dry- and wet-season images were 452.5 g C m⁻² yr⁻¹ with shadow retention and 432.43 g C m⁻² yr⁻¹ with shadow correction.

To investigate if the 2 seasonal images were preferable over the 1 season image, a comparison was made between the annual NPP in Table 6 and the field-measured carbon amount (i.e., 430 g C m⁻² yr⁻¹) in Table 1. Results indicates that a large bias existed in the 1- season image when compared to 430 g C m⁻² yr⁻¹. Therefore, the best estimation of the NPP in this study focused on the dry- and wet-season images because of the smallest bias. However, if the shadow process was considered, then the annual NPP with shadow correction was better than that with shadow retention because there was only a 2.43 g C m⁻² yr⁻¹ difference with the field-measured carbon amount. Figure 5 shows distribution maps of

annual NPP in the dry- and wet-season images with shadow retention and shadow correction.

Analysis of NPP variations from different seasons and forest types

From the above results, the monthly and annual NPP values estimated from the dry- and wet-season images and 2 shadow processes (i.e., shadow retention and shadow correction) were then applied to analyze NPP variations from different seasons and forest types.

NPP variations from different seasons

Since this study focused on NPP estimations in 2003, the following seasonal analysis of NPP variations was based on 4 seasons (spring, summer, autumn, and winter) in 2003. Table 7 shows NPP estimations from the accumulation period and 4 different seasons. Results indicate that most NPP ac-

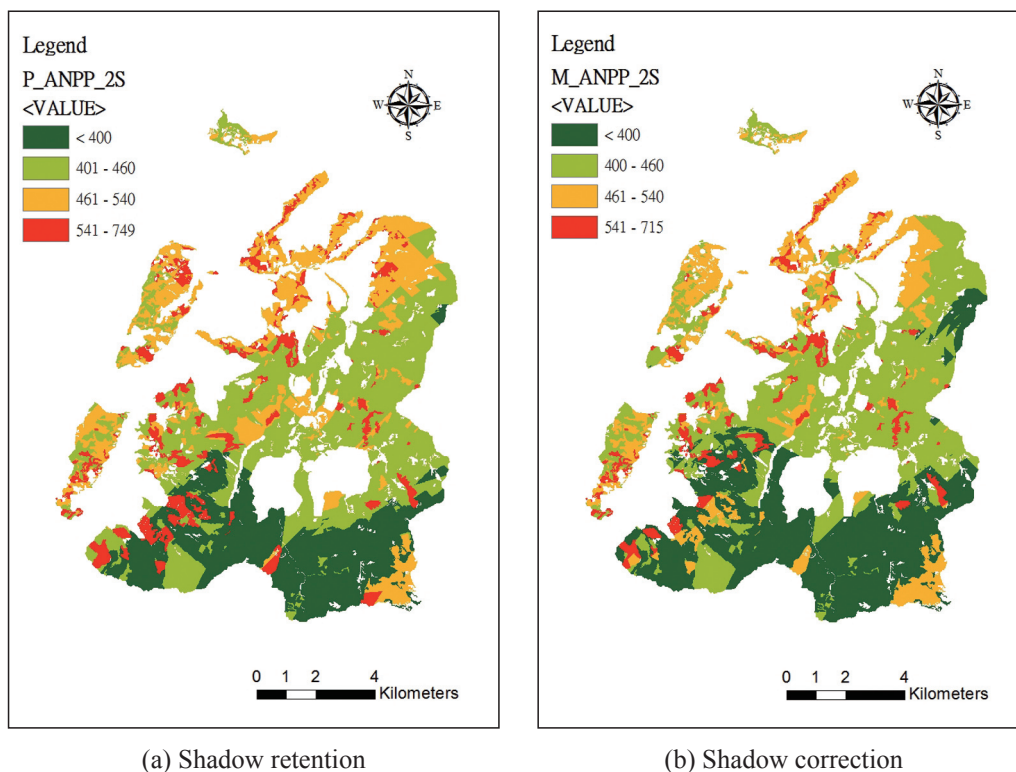


Fig. 5. Distribution maps of annual net primary productivity (NPP) in the dry and wet seasons with (a) shadow retention and (b) shadow correction.

Table 7. Net primary productivity (NPP) variations ($g\ C\ m^{-2}$) from different seasons in 2003

Shadow process	NPP (Jan.~Dec.)	NPP (Apr.~Oct.)	Spring (Mar.~May)	Summer (June~Aug.)	Autumn (Sep.~Nov.)	Winter (Dec.~Feb.)
Shadow retention	452.50	389.28 (86%)	109.78 (24.3%)	191.41 (42.3%)	120.33 (26.6%)	30.99 (6.8%)
Shadow correction	432.43	372.01 (86%)	104.91 (24.3%)	182.92 (42.3%)	114.99 (26.6%)	29.61 (6.8%)

cumulation was distributed between April and October, and it was about 86% of the annual NPP. NPP values in spring, summer, autumn and winter were about 24.3, 42.3, 26.6, and 6.8%, respectively. Obviously, seasonal NPP variations were significant in the study area. The sequence of NPP variation from maximum to minimum was summer, autumn, spring, and winter.

NPP variations from different forest types

Table 8 shows NPP variations from different forest types, and Fig. 5 shows the distribution of NPP spatial variations with shadow retention and shadow correction. Results in Table 8 are reasonable because the NPP with shadow retention was larger than that with shadow correction. Compared to the field-measured carbon amount ($430\ g\ C\ m^{-2}$

Table 8. Net primary productivity (NPP) variations from different forest types in 2003

Forest type	Area (ha)	Annual NPP (g C m ⁻² yr ⁻¹)		Total NPP (10 ⁶ g C yr ⁻¹)		Field-measured carbon amount (10 ⁶ g C yr ⁻¹)
		Shadow retention	Shadow correction	Shadow retention	Shadow correction	
NHMT	5008.13	429.71	410.66	21520.44	20566.39	20433.17
CT	1663.67	411.32	393.08	6843.01	6539.55	6504.95
CMT	927.13	587.72	561.65	5448.93	5207.23	5173.39
CHMT	677.29	497.83	475.75	3371.75	3222.21	3203.58
HMT	853.14	483.70	462.24	4126.64	3943.55	3915.91
Study area	9129.36	452.50	432.43	41310.35	39478.09	39231.00

NHMT, natural hardwood mixed type; CT, conifer type; CMT, conifer mixed type; CHMT, conifer-hardwood mixed type; HMT, hardwood mixed type.

yr⁻¹), the NPP with shadow correction (432.43 g C m⁻² yr⁻¹) was reasonable and acceptable because of the smallest bias. Therefore, the following variation analysis was based on the annual NPP with shadow correction. Clearly, conifer mixed forest had the largest NPP at 561.65 g C m⁻² yr⁻¹ among the 5 forest types. The sequence from maximum to minimum was conifer-hardwood mixed forest, hardwood mixed forest, natural hardwood mixed forest, and conifer forest. However, natural hardwood mixed forest had the largest total NPP at 2.056639 × 10¹⁰ g C yr⁻¹ because of the largest area. Then the sequence was conifer forest, conifer mixed forest, hardwood mixed forest, and conifer-hardwood mixed forest.

This study applied SPOT images and the model of light use efficiency to estimate the NPP of the study area. During the research process, 3 topics of the shadow effect, ϵ_{\max} for forest types, and image acquisition were also investigated. Some discussion related to this study is presented here. First, from results of the generated shadow map and shadow effect on the NDVI and SR, the shadow effect and its process should obviously be considered when using SPOT vegetation indices to estimate the NPP. However, results of the FPAR estimation indicated that the process of

shadow removal cannot be applied because it generated a lower FPAR due to the linear transformation from the NDVI to FPAR_{NDVI}. This finding is seldom seen in NPP studies because most studies use remote sensing images with low spatial resolution such as AVHRR, MODIS images, and their shadow effects are greatly reduced by the low-resolution data (Burgess et al. 1995). Second, as for the parameter of ϵ_{\max} which is important for NPP estimations, this study simulated the ϵ_{\max} for each forest type of the study area according to the calculated T₁, T₂, and W parameters from meteorological data, the estimated APAR parameter from the seasonal image, and the field-measured carbon amount from the forest inventory data. The simulated ϵ_{\max} for forest types was between the value used in the CASA model (0.389 g C MJ⁻¹) and the simulated value by Zhu et al. (2006), and is also consistent with a study by Peng et al. (2000). Meanwhile, the value of NPP estimation using the simulated ϵ_{\max} was close to that of the field-measured carbon amount. Therefore, the simulated result in this study was reasonable and feasible. Third, to estimate the annual NPP, monthly SPOT images are needed. However, this is difficult in Taiwan due to environmental characteristics. In this study, 2

seasonal SPOT images were selected to investigate the effect of image acquisition on NPP estimations. From the comparison between the estimated annual NPP and field-measured carbon amount, results from the dry- and wet-season images were obviously better than that from a 1-season image. In addition, the analysis of NPP variations using dry-wet season images indicated that the majority of NPP accumulation was about 86% of the annual NPP and was mainly distributed between April and October. This result is similar to that of a study by Zhu (2005). From this result, it is feasible to use seasonal images for estimating the NPP in Taiwan.

CONCLUSIONS

This study focused on applying SPOT vegetation indices to estimate the net primary productivity (NPP) of the Nanzhuang National Forest in Taiwan. Due to the problems of the shadow effect, maximum light use efficiency for forest types, and image acquisition in Taiwan, their effects on the estimation of NPP were also investigated in this study. The following conclusions were drawn. First, remote sensing is a timely, feasible, effective, economic, and large-scale approach to estimate forest NPP. Although a slight difference existed between the estimated NPP from SPOT vegetation indices and the field-measured carbon amount from traditional forest inventory data, this technique has advantages in analyzing spatiotemporal variations in NPP. For example, seasonal variations in the NPP were significant at the Nanzhuang National Forest in Taiwan. The majority of NPP accumulation was distributed between April and October, and it was about 86% of the total NPP in a year. Second, the shadow effect and its process should be considered when using SPOT vegetation indices to estimate

the FPAR. We propose that the process of shadow removal cannot be applied when estimating the FPAR because it generates a lower FPAR due to the linear transformation from the NDVI to $FPAR_{NDVI}$ or the SR to $FPAR_{SR}$. Therefore, it is not suitable for estimating values of the FPAR, APAR, and NPP. Third, maximum light use efficiency is an important parameter for NPP estimation when using remote sensing techniques. However, many divergences still exist as to values of different forest types. This study simulated the maximum light use efficiency for each forest type according to the calculated temperate scalars and water scalar, the estimated APAR from remote sensing data, and the field-measured carbon amount from forest inventory data. The simulated result was feasible when comparing the estimated NPP with the field-measured carbon amount. Fourth, monthly images are important for accurately estimating the annual NPP, in addition to the shadow effect and maximum light use efficiency of forest types. Because it is difficult to acquire monthly images in Taiwan, an alternative approach using the dry-wet season images was adopted. From the analysis of NPP variations and a comparison between the estimated NPP and field-measured carbon amount, the proposed approach is feasible for estimating NPP of forests in Taiwan.

ACKNOWLEDGEMENTS

The author sincerely appreciates the Taiwan Forest Bureau and Taiwan Typhoon and Flood Research Institute for respectively providing the forest inventory data and meteorological data. Specifically, thanks are due to the Ministry of Science and Technology, Taiwan for financial support (NSC101-2410-H-034-042) and Taiwan Forestry Research Institute for the study support in a sabbatical year.

LITERATURE CITED

- Burgess AW, Lewis P, Muller JPAL. 1995.** Topographic effects in AVHRR NDVI data. *Remote Sens Environ* 54:223-32.
- Field CB, Randerson JT, Malmström CM. 1995.** Global net primary production: combining ecology and remote sensing. *Remote Sens Environ* 51:74-88.
- Goetz SJ, Prince SD. 1996.** Remote sensing of net primary production boreal forest stands. *Agric For Meteorol* 78:149-79.
- Gower ST, Kucharik CJ, Norman JM. 1999.** Direct and indirect estimation of leaf area index, fAPAR, and net primary production of terrestrial ecosystem. *Remote Sens Environ* 70:29-51.
- Hatfield JL, Asrar G, Kanemasu ET. 1984.** Intercepted photosynthetically active radiation in wheat canopies estimated by spectral reflectance. *Remote Sens Environ* 14:65-75.
- IPCC. 2003.** Good practice guidance for land use, land-use change and forestry. Hayama, Japan: International Panel on Climate Change (IPCC)/IGES. 632 p.
- Law BE, Waring RH. 1994.** Combining remote sensing and climatic data to estimate net primary production across Oregon. *Ecol Appl* 4(4):717-28.
- Los SO, Justice CO, Tucker CJ. 1994.** A global 1° by 1° NDVI dataset for climate studies derived from the GIMMS continental NDVI data. *Int J Remote Sens* 15:3493-518.
- Monteith JL. 1972.** Solar radiation and productivity in tropical ecosystem. *J Appl Ecol* 9:747-66.
- Peng SL, Guo ZH, Wang BS. 2000.** Use of GIS and RS to estimate the light utilization efficiency of the vegetation in Guangdong, China. *Acta Ecol Sin* 20(6):903-9. [in Chinese].
- Potter CS, Randerson JT, Field CB. 1993.** Terrestrial ecosystem production: a process model based on global satellite and surface data. *Global Biochem Cycle* 7:811-41.
- Raymond E, Hunt JR. 1994.** Relationship between woody biomass and PAR conversion efficiency for estimating net primary productivity from NDVI. *Int J Remote Sens* 15:1725-30.
- Ruimy A, Saugier B. 1994.** Methodology for the estimation of terrestrial net primary production from remotely sensed data. *J Geophys Res* 97:18515-21.
- Sellers PJ. 1985.** Canopy reflectance, photosynthesis, and transpiration. *Int J Remote Sens* 6:1335-71.
- Wang JM. 2007.** A study on the estimative approach of forest carbon sequestration for national forest land in Taiwan. Master's thesis. Taipei, Taiwan: National Taiwan Univ. 148 p.
- Wang RY. 2010.** A study on the carbon stocks of varied forest types by using satellite imagery—the case of Nanjhuang working circle in Hsinchu Forest District. PhD dissertation. Taipei, Taiwan: Chinese Cultural Univ. 168 p.
- Zhou W, Huang G, Troy A, Cadenasso ML. 2009.** Object-based land cover classification of shaded areas in high spatial resolution imagery of urban areas: a comparison study. *Remote Sens Environ* 113:1769-77.
- Zhu WQ. 2005.** Estimation of net primary productivity of Chinese terrestrial vegetation based on remote sensing and its relationship with global climate change. PhD dissertation. Beijing, China: Beijing Normal Univ. 163 p.
- Zhu WQ, Pan YH, Hao HE, Deyon YU, Haibo HU. 2006.** Simulation of maximum light use efficiency for some typical vegetation types in China. *Chin Sci Bull* 51(4):457-63.